HHS Public Access

Author manuscript

Nature. Author manuscript; available in PMC 2019 May 22.

Published in final edited form as:

Nature. 2018 October ; 562(7726): 286–290. doi:10.1038/s41586-018-0568-2.

Crystal structure of a membrane-bound *O*-acyltransferase

Dan Ma[1], **Zhizhi Wang**[1], **Christopher N. Merrikh**[2], **Kevin S. Lang**[2], **Peilong Lu**[3], **Xin Li**[1,4], **Houra Merrikh**[2,5], **Zihe Rao**[4,6,7,8,9], and **Wenqing Xu**[1,6,*]

[1.] Department of Biological Structure, University of Washington, Seattle, WA, USA.

[2.] Department of Microbiology, University of Washington, Seattle, WA, USA

[3.] Department of Biochemistry, University of Washington, Seattle, WA, USA

[4.] College of Life Sciences, State Key Laboratory of Medicinal Chemistry Laboratory, Nankai University, Tianjin, China

[5.] Department of Genome Sciences, University of Washington, Seattle, WA, USA

[6.] National Laboratory of Biomacromolecules, CAS Center for Excellence in Biomacromolecules, Institute of Biophysics, Chinese Academy of Sciences, Beijing, China.

[7.] Shanghai Institute for Advanced Immunochemical Studies, ShanghaiTech University, Shanghai, China

[8.] University of Chinese Academy of Sciences, Beijing, China.

[9.] Laboratory of Structural Biology, School of Medicine, Tsinghua University, Beijing, China.

Abstract

Membrane-bound *O*-acyltransferases (MBOATs) represent a superfamily of integral transmembrane enzymes found in all kingdoms of life[1]. In bacteria, MBOATs modify protective cell surface polymers. In vertebrates, some MBOAT enzymes such as acyl-CoA:cholesterol acyltransferase (ACAT) and diacylglycerol acyltransferase 1 (DGAT1) are responsible for lipid biosynthesis and phospholipid remodeling[2,3]. Some other MBOATs, including porcupine (PORCN), hedgehog acyltransferase (HHAT) and ghrelin acyltransferase (GOAT), catalyze essential lipid modifications of secreted proteins such as Wnt, hedgehog and ghrelin, respectively[4–10]. Although many MBOAT proteins are important drug targets, little is known about their molecular architecture and functional mechanisms. Here we present crystal structures of DltB, a MBOAT responsible for D-alanylation of cell wall teichoic acid (TA) of Gram-positive bacteria[11–16], by itself and in complex with the D-alanyl donor protein, DltC. DltB contains a ring

* Corresponding wxu@uw.edu.

Author Contributions

D.M. did protein purification, crystallization, and related binding and enzymatic analysis. D.M. and Z.W. collected diffraction data and determined the crystal structure. Z.W. did structural refinement. C.N.M. constructed the *B. subtilis* strains, and C.N.M., K.S.L. and H.M. performed the cell survival assays. P.L. contributed to molecular cloning and sample preparation. X.L. and Z.R. contributed to screening of some other MBOAT proteins. D.M., Z.W. and W.X. analyzed structural data and wrote the paper. All authors participated in manuscript revision and analysis of biochemical data.

The authors declare no competing financial interests.

of 11 peripheral transmembrane helices, which shield a highly conserved extracellular structural "funnel" extending into the middle of lipid bilayer. The conserved catalytic histidine residue is located at the bottom of this funnel and connected to the intracellular DltC through a narrow tunnel. Mutation of either the catalytic histidine or the DltC binding site of DltB abolishes LTA D-alanylation, and sensitizes the Gram-positive bacterium *Bacillus subtilis* to cell wall stress, suggesting cross-membrane catalysis involving the tunnel. Structure-guided sequence comparison among DltB and vertebrate MBOATs reveals a conserved structural core and suggests similar catalytic mechanisms. Our structures provide a template for understanding MBOAT structure-function relationships and for developing therapeutic MBOAT inhibitors.

Keywords

Membrane-bound *O*-acyltransferase; MBOAT; transmembrane enzyme; DltB; DltB-DltC complex; crystal structure; antibiotic; Wnt; hedgehog; ghrelin

MBOAT proteins in the MBOAT superfamily (http://pfam.xfam.org/family/MBOAT; >7,000 members) perform divergent functions with distinct substrate preferences, although many of them use acyl-CoA as the acyl-group donor (Extended Data Fig. 1). Among bacterial MBOATs, DltB is essential for D-alanylation of cell wall teichoic acids[11–16], which are important for growth, biofilm formation, adhesion and virulence of Gram-positive bacterial pathogens. To understand the molecular mechanisms of MBOAT proteins, we have determined the crystal structure of full-length DltB from *S. thermophilus* at 3.3 Å resolution (Fig. 1, Extended Data Figs. 2, 3, and Extended Data Table 1). DltB contains 415 residues, arranged into 17 helices, with both N- and C-termini in the extracellular space (Fig. 1a). Except for the short N- and C-terminal helices, all other 15 helices are mostly within the lipid bilayer. Among them, 11 transmembrane helices form an external ring-shaped ridge, and shield a central basin that is thinner than the lipid bilayer (Fig. 1, Extended Data Fig. 4). The thin central area results from an intracellular concave surface and a more dramatic extracellular structural funnel (Fig. 1d). Since they are more conserved than the peripheral ring helices among MBOAT proteins and are likely involved in catalysis (see below), we refer to structural components in this thin central area as the MBOAT central core. The DltB 3D structure can be roughly divided into 3 parts: N-terminal helical ridge (N-ridge), central core, and C-ridge (Extended Data Fig. 4). A Dali search using our DltB structure did not find any protein with a similar fold.

The extracellular side of DltB forms a structural funnel, which is extended into the middle of lipid bilayer (Fig. 1d). The surface inside the funnel is formed by residues from multiple transmembrane helices and loops. Strikingly, in sharp contrast to the low-conservation of residues forming the outer ridge surfaces, these residues are extremely conserved among DltB proteins (Fig. 1e, Extended Data Fig. 5). Importantly, previous studies have shown that a histidine residue strictly conserved in all confirmed MBOAT proteins is likely involved in catalysis. Mutation of the corresponding histidine residue in all tested MBOATs (PORCN, HHAT, GOAT, DGAT and ACAT) either abolished or substantially reduced the acyltransferase activities of corresponding MBOATs[17–22]. In our DltB structure, this histidine residue (His336, last residue of helix H14) is located at the bottom of the

extracellular funnel (Fig. 1d, f). Another highly conserved histidine residue (His289) in the MBOAT superfamily[1] is also located at the bottom of this funnel and spatially close to His336 (Extended Data Fig. 3). Our crystal structure and the structural conservation strongly suggest the importance of this extracellular funnel in DltB activity.

Interestingly, four *S. aureus* DltB mutations, corresponding to *S. thermophilus* DltB mutants S165T, A209D, F250L and F250I, have been identified to be resistant to DltB inhibitors amsacrine and *o*-AMSA[14]. Ser165, Ala209 and Phe250 are spatially located at the surface of the funnel, with Ser165 and Phe250 sitting near the bottom of funnel and close to His336 (Fig. 1f). We predict that amsacrine and *o*-AMSA bind in this DltB funnel, and the abovementioned four mutations may abolish inhibitor binding. We speculate that this funnel may be involved in extracellular TA substrate binding or play other key roles in catalysis. Given the biological importance of DltB[14] and the dramatic conservation of the DltB extracellular funnel surface, DltB inhibitors binding to this funnel may serve as wide-spectrum antibiotics against Gram-positive bacteria.

In addition to its role in D-alanylation, DltB also plays a role in host-pathogen interactions. A missense mutation in *S. aureus* DltB (T113K) is sufficient to convert a *S. aureus* strain from a human-specific pathogen to a rabbit specific pathogen, without any change in LTA D-alanylation level[23]. Strikingly, Thr113, as well as all other ten *S. aureus* DltB residues associated with host specificity change are located at a non-conserved extracellular apex (Extended Data Figs. 4d, 5). This unusual feature strongly suggests that DltB from *S. aureus* and potentially some other species may interact with one or more unknown host factors using their extracellular ridges.

In the Dlt-mediated D-alanylation system, to serve as the D-alanyl group donor to TA, DltC first needs to be modified with the Ppant group at Ser35, which can be catalyzed by the acyl carrier protein synthase (AcpS). The Ppant-modified DltC can be further modified with a D-alanyl group by DltA, through a thioester bond (Fig. 2a). To test if DltB can directly interact with DltC, we co-expressed His-tagged AcpS and a GST-tagged DltC, and purified DltC, which appears uniformly Ppant-modified as confirmed by mass spectrometry (Extended Data Fig. 2b, c). Using GST-pulldown and SEC analysis, we found that DltC(Ppant) and DltB form a tight complex (Fig. 2b). Octet binding analysis showed a *K*d of 0.26 μM between DltB and DltC(Ppant) (Extended Data Fig. 6). In contrast to the tight DltB-DltC interaction, DltB does not form a detectable complex with DltA or the extracellular domain of DltD, and there is no detectable interaction between DltA and DltC on the cytoplasmic side (data not shown).

To understand how DltB functions as a MBOAT, we also determined the crystal structure of the DltB-DltC(Ppant) complex at 3.15 Å resolution (Fig. 2c). Cytoplasmic DltC contains four helices, with Ppant-bonded Ser35 being the first residue of helix 3 (α3). Residues in DltC α3 and the long-loop between α3 and α4 (α3-α4 loop) form the DltB binding surface. DltC interacts mainly with the C-terminal half of DltB H13 and the N-terminal end of DltB H14. This region is formed by a DltB-specific insertion that is missing in other MBOAT proteins[1]. The DltB-DltC interface is mostly hydrophobic, formed by DltB residues Met302, Val305, Ile306, Met309 and DltC residues Met36, Val39, Val43, Val55. In addition, Arg317,

the first residue of H14, forms charged hydrogen bonds with DltC Glu40, whereas the phosphate group of Ser35-Ppant is in a position to form a weak salt bridge with the DltB Lys282 in helix H12 (Fig. 2d, Extended Data Figs. 5, 7). DltB has essentially identical structures in its apo- and DltC-bound states (Extended Data Fig. 7a).

To validate the DltB-DltC interface, we purified DltB mutants V305D and V305D/I306D as well as DltC mutants V39D and V39R, and tested their interactions with their corresponding WT partner using GST-pulldown and Octet assays (Fig. 2b, Extended Data Fig. 6). While DltB V305D substantially reduced WT DltC binding, the DltB V305D/I306D mutant completely abolished DltB-DltC binding. Similarly, both DltC V39D and V39R mutants substantially reduced their ability to interact with DltB. These mutagenesis analyses demonstrate DltB Val305, Ile306 and DltC Val39 are critical for DltB-DltC interaction, and confirm our structural observation that these surface residues are at the DltB-DltC core interface.

There is roughly a straight tunnel between the bottom of the extracellular funnel and the cytoplasmic side. This tunnel is formed by three DltB helices from the C-ridge (H13-H15) and the small horizontal helix H12 from the central core. DltB residues inside the tunnel are highly conserved among DltB proteins (Fig. 3a, Extended Data Fig. 5), and also bear conservation in other MBOAT proteins (see below), suggesting that this tunnel is functionally important. It should be noted that in our current DltB and DltB-DltC complex structures, the sidechain of the conserved Trp285 from helix H12 keeps this tunnel in a closed conformation (Fig. 3a, Extended Data Fig. 7c). We speculate that the DltB conformation we captured is in a “resting” state of the DltB enzyme.

One striking feature of the DltB-DltC complex is that Ser35 is located at the cytoplasmic entrance of the tunnel (Fig. 3b). Consistent with a “resting” state conformation, while the electron density for the Ppant phosphate group is well defined in our electron density map, density for the rest of Ppant chain is too thin for model building. Consistently, Octet analysis showed that the DltC-S35A mutant can also interact with DltB with similar affinity (*K*d ~0.19 μM), indicating that the Ppant group is not essential for DltB-DltC interaction. The Ppant group can potentially switch between occupying the tunnel and being flexible in the cytoplasmic open space, since the Ser35 phosphate group is positioned between the tunnel entrance and the open cytoplasmic space. While the most conserved His336 is located at the C-terminus of the DltB H14 helix, DltC makes contacts with the C-terminal half of the H13 helix and the N-terminus of the H14 helix, suggesting that the distance between DltC Ser35 and DltB His336 may be largely fixed without conformational changes involving DltB helix H13 and/or H14.

To examine the functional significance of the tunnel, we generated *B. subtilis* strains lacking the *dlt* operon, and then complemented with a heterologous copy of the *dlt* locus expressed from its native promoter. Both the LTA D-alanylation level and cell viability of *dlt*-deleted *B. subtilis* cells complemented with either WT or various mutant *dltB* were evaluated using a ^{14}C-D-Ala radiolabeling and lysozyme-sensitivity assays, respectively. Mutation of DltB residues corresponding to *S. thermophilus* DltB His336 or the DltC binding site completely abolished LTA D-alanylation (Fig. 3c). In addition, both mutations significantly reduced *B.*

subtilis viability in the presence of lysozyme, while mutations of two other DltB residues did not have significant effect in both assays (Fig. 3c, d, Extended Data Fig. 8). Our functional assay data and structural features of DltB together strongly suggest that the tunnel is important for the catalytic mechanism of DltB (Fig. 3e).

In some other *O*-acyltransferases such as carnitine acyltransferase[24], a conserved histidine catalyzes the acyl transfer reaction by aligning the carnitine substrate with the acyl-CoA thioester bond. The Ppant-D-Ala chain has a length of ~20 Å between the phosphate group and D-Ala. In our crystal structure, the distance between the Ser35-Ppant phosphate group and His336 is ~21 Å. Should the tunnel be open for the Ppant-D-Ala chain binding, this distance would allow His336 to align the acyl-group receiving substrate (likely a glycerol phosphate unit within LTA molecule) with D-alanylated DltC(Ppant). Thus, our structures suggest a model in which D-alanylation of LTA occurs between the LTA bound to the extracellular funnel and the D-alanyl group on DltC(Ppant-D-Ala) bound to the cytoplasmic side of tunnel (Fig. 3e).

Since DltB forms a stable complex with DltC(Ppant) even without the D-alanyl group, and the DltC Ser35 is open to the cytosol, we speculate that DltC(Ppant) forms a constitutive complex with DltB during catalysis, and the Ppant chain can migrate between tunnel and cytosol where loading of the D-alanyl group of DltC(Ppant) can be catalyzed by DltA. How does the DltB tunnel open for Ppant binding? The DltB tunnel is formed by the small horizontal helix H12 and the long transmembrane helices (H13-H15) forming the C-ridge of DltB. Compared to the DltB C-ridge helices, helix H12 is more likely to be the mobile structural component. The tunnel opening can be caused by movement or a conformational change of the short helix H12, the position of which is stabilized through local hydrophobic interactions. H12 may change its position without disturbing the N- and C-ridge structures and lead to the opening of the tunnel. H12 movement may be induced by the presence of an appropriate signal, such as substrate binding with the extracellular funnel and/or binding of intracellular ligands such as DltC(Ppant-D-Ala). Here it should be noted that in the *dlt* system, DltD is required for LTA D-alanylation *in vivo*. It remains unclear how DltD may contribute to this process. A combination of structural and enzymatic analysis is needed to reveal the role of DltD and detailed catalytic mechanism of DltB.

What is the implication of the DltB structure to other MBOAT proteins? Despite a low overall sequence homology, a more conserved region within MBOAT sequences, termed MBOAT2 homology, was identified (http://pfam.xfam.org/family/MBOAT_2). The MBOAT2 homology covers the sequences corresponding to the DltB region from DltB H12 to the N-terminus of H15 (Fig. 1b), which forms majority of the central core that is thinner than the lipid bilayer. Thus the thin central core and the extracellular/lumen funnel are likely common structural features of many MBOATs. It has been demonstrated that the most conserved histidine (DltB His336), which is located within this MBOAT2 homology domain, is critical for enzymatic activities of all tested MBOAT proteins, including PORCN, HHAT, GOAT, ACAT, and DGAT[17–22], strongly suggesting a common or similar catalytic mechanism for the MBOAT superfamily of proteins. The conserved extracellular/lumen structural funnel, the thin central core, and the tunnel we observed in our DltB structure, are likely shared by many other MBOATs. Indeed, our DltB crystal structure is in remarkable

agreement with the membrane topology models of HHAT and GOAT previously derived from biochemical data[25–27] (Extended Data Fig. 9). For example, in each case, the catalytic histidine was predicted to be at the end of a HHAT/GOAT transmembrane helix facing the lumen side, in perfect agreement with our DltB structure. It is also consistent that the critical horizontal helices H11-H13 in our DltB core structure were predicted to be a long cytoplasmic HHAT/GOAT region/subdomain. In addition, a predicted “reentrant helix” observed in both HHAT and GOAT nicely corresponds to the H7-H8 “half-way turn-back” structure in the DltB central core (Fig. 1b, Extended Data Fig. 9). In contrast to the similarity in the core structure, the N- and C-terminal regions of HHAT and GOAT are much more divergent.

Among vertebrate MBOATs, PORCN and GOAT are responsible for lipid modifications of secreted Wnts and ghrelin, respectively. They all catalyze reactions across ER-membrane with the acyl group accepting proteins located in the ER lumen and acyl-CoA in the cytosol[6,7]. Since DltB also catalyzes cross-membrane reactions, we examined the sequence homology among DltB, PORCN and GOAT. It appears that there are four conserved regions: the region covering DltB helices H12-H14 (the MBOAT2 homology region), the DltB H7-H8 region, and two partial helices in the inner circle of the DltB structure (most of helix H6 and the central part of helix H10) (Fig. 4, Extended Data Fig. 9). Therefore, while sequences encoding the N- and C-ridges of DltB are generally not conserved in other MBOATs, the central core of DltB, along with its structural neighbors in the inner circle (e.g. parts of helices H6 and H10), are conserved among vertebrate MBOATs including PORCN, and GOAT. We suggest that the non-conserved nature of the ridges allow for recognition of distinct substrates specific to different members within the MBOAT family. It should be noted that binding of acyl-CoA as acyl group donors for most metazoan MBOATs is likely very different from the mechanism for DltB which uses DltC(Ppant-D-Ala) as the acyl-donor.

The deep, conserved DltB extracellular structural funnel, as well as the DltB tunnel, may be an excellent target for drug development. Furthermore, many other bacterial and metazoan MBOATs may also be very druggable, as many of them are present on cell membrane surface. In addition, the deep extracellular/lumen funnel shape close to the active site is likely a conserved feature for many MBOATs, which may be excellent drug binding sites. Indeed, even in the absence of a 3D structure and detailed enzymatic analysis using purified PORCN, multiple small-molecule inhibitors with IC_{50} in low nM range have been found through cell-based screening and some of them have been used in anti-cancer clinical trials[28–30]. Potent HHAT and GOAT inhibitors have also been reported and examined in multiple studies[5]. Based on our crystal structures, we predict that many more highly-potent MBOAT inhibitors will be discovered in the future.

3D structural prediction for MBOAT proteins has been very difficult and unreliable. Our DltB crystal structures serves as a cornerstone for understanding structures and functions of MBOAT proteins. In addition, our structures reveal an intriguing mechanism for cross-membrane catalysis, and provide a platform for the development of new clinically relevant drugs across species.

Methods

Protein preparation

The cDNA of full-length *S. thermophilus* DltB was subcloned into pET21b (Novagen). cDNAs of *S. thermophilus* AcpS, DltA and DltC were subcloned into pQLink vectors (Addgene) with AcpS and DltA bearing N-terminal 6xHis-tag, and DltC bearing N-terminal GST-tag. *E. coli* strain C43 (DE3) was used for protein overexpression. Overexpression of above proteins was induced by 0.4 mM isopropyl β-d-thiogalactoside (IPTG) when cell density reached OD_{600} of 1.0. After induction at 37 °C for 5 h, the cells were collected, homogenized in buffer containing 25 mM Tris-HCl pH 8.0 and 150 mM NaCl.

For DltB purification, after disruption by sonication, cell debris was removed by centrifugation for 10 min at 20,000 g. The supernatant was collected and ultracentrifuged for 1.5 h at 100,000 g. Membrane fraction was collected and homogenized with buffer containing 25 mM Tris-HCl pH 8.0 and 150 mM NaCl. n-Decyl-β-D-Maltopyranoside (DM; Anatrace) was added to the membrane suspension to a final concentration of 1.5% (w/v) and then incubated for 2 h at 4 °C. After another ultracentrifugation step at 100,000g for 30 min, the supernatant was collected and loaded onto Ni-NTA affinity resin (Ni-NTA; Qiagen). Followed by wash with buffer containing 25 mM Tris-HCl pH 8.0, 500 mM NaCl, 25 mM imidazole and 0.2% (w/v) DM, DltB was eluted with buffer containing 25 mM Tris-HCl pH 8.0, 150 mM NaCl, 400 mM imidazole and various detergents from Anatrace. After being concentrated to 10 mg/ml, DltB was further purified by gel filtration (Superdex-200 10/30; GE Healthcare). The buffer for gel filtration contained 25 mM Tris-HCl pH 8.0, 150 mM NaCl and various detergents. The peak fractions were collected.

For DltA and DltC purification, after sonication, cell debris was removed by centrifugation for 1 h at 35,000 g. The supernatant was loaded onto Ni-NTA affinity resin and Glutathione Sepharose 4 resin (GS4B resin, GE Healthcare) respectively. After wash step, N-terminal GST-tag was either removed from DltC or kept unremoved according to different experiment purpose. After elution, DltA and DltC solutions were loaded onto HiTrap Q HP columns (5 ml; GE Healthcare), and protein samples eluted from Q column were further purified by gel filtration. Peak fractions were collected and concentrated. Finally, DltA and DltC were in buffer containing 25 mM Tris-HCl pH 8.0 and 150 mM NaCl.

DltB and DltC mutants were generated with a standard PCR-based strategy and were subcloned, overexpressed and purified in the same way as the wild-type proteins.

Protein crystallization

The hanging-drop vapor-diffusion method was performed at room temperature during crystallization. DltB and DltC proteins were purified as mentioned above, and crystals were obtained with DltB purified with n-Nonyl-β-D-Glucopyranoside (β-NG; Anatrace). For DltB and DltC complex crystallization, DltB and DltC were purified separately and mixed before crystallization at molar ratio of 1:2. Crystals belonging to crystal form I (space group $P2_1$, Extended data Table 1) were crystallized in buffer containing 21% PEG400, 100 mM Tris-HCl pH 7.5, 100 mM NaCl, and 100 mM $MgCl_2$. Crystals belonging to crystal form II (space group $P2_1$, Extended data Table 1) were crystallized in buffer containing 27%

PEG400, 100 mM sodium citrate pH 5.6, 200 mM $NH_4H_2PO_4$, and 100 mM $(NH_4)_2SO_4$. Crystals belonging to crystal form III (space group $P2_12_12_1$, Extended data Table 1) were crystallized in buffer containing 27% PEG400, 100 mM HEPES pH 7.5, 200 mM sodium citrate tribasic dihydrate and 3% 1,5-diaminopentane dihydrochloride. For crystals in different crystal forms above, thin or thick rod-shaped crystals typically grew for 1 to 2 weeks to full crystal size. Gold derivatives were obtained by soaking the crystals in crystal form I for 2 h in mother liquor containing 2 mg/ml $KAu(CN)_2$.

Data collection and structure determination

The crystals were directly flash-frozen in liquid nitrogen. Screening and data collection were performed at the Advanced Light Source (ALS), beamlines 5.0.1, 8.2.1 and 8.2.2. All diffraction data were processed by HKL2000[31]. The single-wavelength anomalous dispersion (SAD) data set was collected near the gold L-III absorption edge at a wavelength of 1.02 Å (Extended Data Table 1). The gold derivative sites and the initial phases were determined by PHENIX[32]. Twenty gold derivative sites were found in one asymmetric unit, and the experimental electron density map clearly showed the presence of four DltB molecules in one asymmetric unit. The *B. subtilis* DltC crystal structure (PDB 4BPH) was used as the searching model for our DltC molecules[33]. The complex model was improved using iterative cycles of manual rebuilding with the program COOT[34] and refinement with a native dataset of 3.30 Å using Refmac5 of the CCP4 7.0 program suite[35]. The structures for crystal forms II and III were solved by molecular replacement using the model from crystal form I. All structure model figures in the paper were generated using Pymol[36]. The protein conservation surface was generated using the ConSurf server[37], based on the alignment of DltB sequences generated using T-Coffee[38].

Binding assay

Pull down assays were performed as described below. 10 μg of wild-type DltB (or DltB mutants), 20 μg of wild-type GST-DltC (or GST-DltC mutants) and 10 μl GS4B resin were mixed in 100 μl of pull down buffer containing 25 mM HEPES pH 7.5, 150 mM NaCl and 0.15% (w/v) DM. The mixed samples were incubated at 4 °C on a rotisserie for 1 h, followed by washing the resin with pull down buffer for 3 times. During each wash, 100 μl of pull down buffer was added to each sample and incubated at room temperature for 2 min before centrifugation and removal of supernatant. After wash, resin samples were analyzed by SDS-PAGE, with Coomassie Blue staining.

Binding assays were also performed at room temperature using Octet system (FortéBio). Free GST, and GST-tagged WT DltC or DltC mutants were mobilized on anti-GST biosensors (FortéBio). After quenching with free GST to block free antibody sites on biosensors, the biosensors were dipped into DltB solutions for binding measurement. The concentration gradient of DltB used in Octet binding assay is: 0.03 μM, 0.1 μM, 0.3 μM, 1 μM, 3 μM, 10 μM.

B. subtilis strain construction for functional assays

The *cat* gene was PCR amplified from pGEMcat, while 500bp upstream and downstream of *dlt operon* fragments were amplified from the *B. subtilis* genome. These three pieces were

assembled using isothermal assembly and transformed directly into *B. subtilis* HM1 strain, resulting in *dlt* operon deleted *B. subtilis*. The deletion was confirmed by PCR amplification and Sanger sequencing.

Natural *dlt* locus was amplified and cloned into pMMB752. Mutations of *dltB* gene in pMMB752 carrying *dlt* operon and FLAG-tagged constructs were generated base on standard PCR method, followed by isothermal assembly to ligate the ends together. The pMMB752 constructs were transformed into *B. subtilis* with the *dlt* operon deleted from its native locus to generate strains for use in assays.

Detection of LTA D-alanylation

This assay was established base on a previously reported method[14]. WT *B. subtilis* HM1 strain, and *dlt* operon deleted *B. subtilis* HM1 strain complemented with either empty pMMB752 vector or vectors containing natural *dlt* operon bearing mutations on *dltB* gene (untagged or FLAG-tagged) were inoculated from fresh colonies on plate into liquid LB medium supplemented with 0.5 μg/ml erythromycin. Overnight cultures were diluted into 3 ml of LB at OD_{600} of 0.1 and grew to OD_{600} of 0.6. Cells were pelleted and resuspended into 1.5 ml of assay medium containing 0.25x LB, 50 mM Bis-Tris pH 6.0, and 200 μg/ml D-cycloserine. To test the inhibition of amsacrine on LTA D-alanylation for WT *B. subtilis*, final concentration at 150 μM of amsacrine (Abcam) was supplemented into assay medium. After incubation in assay medium for 30 min, ^{14}C-D-alanine (Moravek Biochemicals Inc) was added to final concentration of 25 μM for additional incubation of 30 min or 120 min. Cells were pelleted and resuspended with SDS-loading buffer, following with a freeze/thaw cycle. Samples were vortexed and boiled for 5 min before loading onto 4–20% gradient Tris/glycine gel (Bio-Rad). Gels were dried and exposed to a phosphor storage screen for 3 days before imaging with Typhoon FLA 9000 gel imaging scanner (GE Healthcare).

To compare the expression level of C-terminal FLAG-tagged DltB in corresponding *B. subtilis* strains, each strain was cultured in 1 liter LB to OD_{600} of 0.6. Cells were harvested and disrupted with French press, and cell membrane was isolated by ultracentrifugation after removing cell debris by low speed centrifugation. Membrane of each strain was resuspended with buffer containing 25 mM Tris-HCl 8.0, 150 mM NaCl into 500 μl, followed by freezing at −80 °C. 1 μl of each membrane sample was run onto SDS-PAGE and the expression of FLAG-tagged DltB was detected by western blotting.

Survival assays

Dlt knockout strains of the Gram-positive bacterium *B. subtilis* are sensitive to the cell wall degradative enzyme lysozyme[39]. *B. subtilis* strains were struck on LB plates (supplemented with the appropriate antibiotic when needed) from freezer stocks and incubated overnight at 37 °C. The resulting growth on plates was used to inoculate 2 ml LB broth cultures in glass tubes. The cultures were grown at 37 °C with shaking (260 RPM) to OD_{600} = 1.0 – 2.0. All of the cultures were adjusted to an OD of 0.3 and then serially diluted in LB broth with 10-fold dilutions. For each strain, 5 μl of each dilution was plated onto LB plates and LB plates supplemented with 30 μg/ml of lysozyme (Fisher) and incubated at 30 °C overnight. After

incubation, colonies were enumerated and plates were imaged with a Bio-Rad Gel Doc XR+ Molecular Imager.

Data availability

Atomic structures have been deposited in the Protein Data Bank (PDB) with accession codes 6BUG (crystal form I), 6BUH (crystal form II) and 6BUI (crystal form III). All other data that support the findings of this study are available from the corresponding author upon reasonable request.

Extended Data

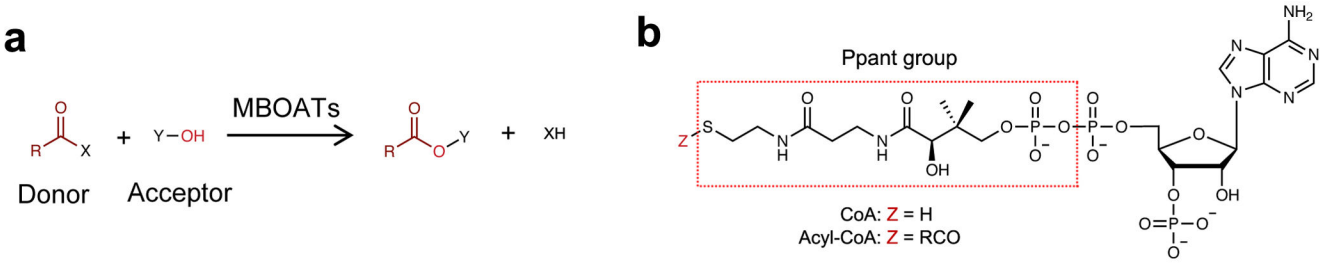

c

MBOAT	Acyl-group Donor	Acyl-group Acceptor
Porcupine	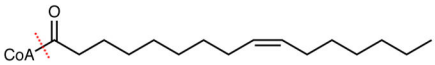	Wnt-Ser209-OH
GOAT	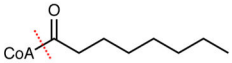	Ghrelin-Ser3-OH
DGAT1	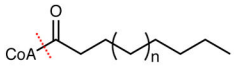	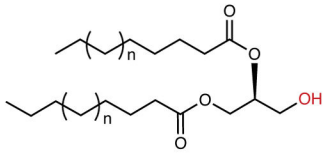 Diacylglycerol
ACAT	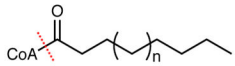	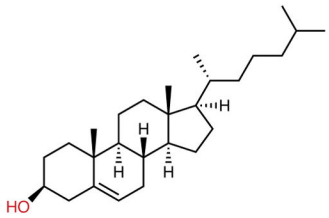 Cholesterol
DltB	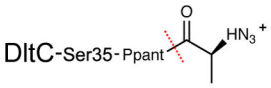	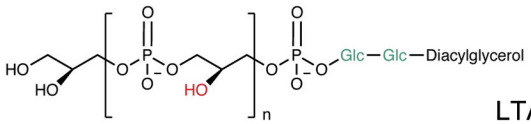 LTA

d

Extended Data Figure 1 |. MBOAT catalyzed reactions and chemical structures of MBOAT substrates.

a, General reaction catalyzed by MBOATs. **b,** Structure of CoA/acyl-CoA. The red rectangle highlights the 4'-phosphopantetheinyl prosthetic (Ppant) group within CoA structure. For known acyl group donors of MBOATs, acyl groups are covalently linked with the sulfhydryl group of Ppant of acyl-CoA or other molecule. **c,** Comparison of acyl-group donors and acceptors of Porcupine, GOAT, DGAT1, ACAT and DltB. In the column of acyl-group donors, the red dash lines indicate the bonds which are broken during acyl transfer reactions. In the column of acyl-group acceptors, the hydroxyl groups which accept acyl groups are

indicated with red color. ACAT½ and DGAT1 utilize saturated and unsaturated long-chain acyl-CoA. **d,** Reaction catalyzed by DltB. DltB catalyzes D-alanylation of both WTA and LTA. Since WTA D-alanylation is at least partially dependent on LTA D-alanylation, here we only discuss D-alanylation of LTA. DltB transfers D-alanyl groups onto hydroxyl groups of polyglycerolphosphate chain of LTA molecule. For simplicity, only the type I LTA structure is shown here. The fatty acid chains are responsible for anchoring of LTA to membrane of Gram-positive bacteria.

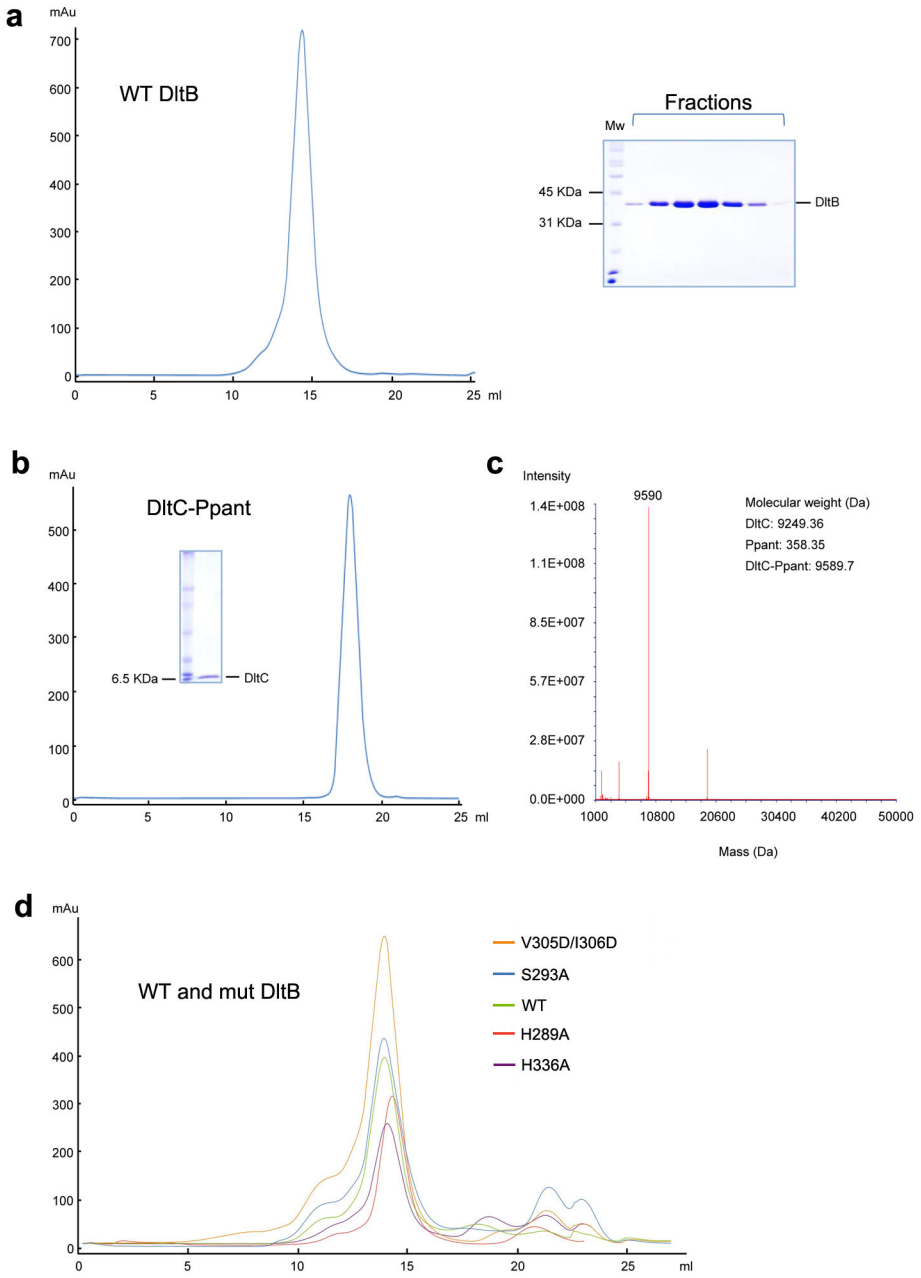

Extended Data Figure 2 |. Purification of DltB, DltC(Ppant) and DltB mutants.

a, Gel Filtration result of DltB. DltB can be purified into homogeneity in most detergents and is well behaved during gel filtration chromatography (SEC). **b,** SDS-PAGE and SEC profile of DltC. **c,** Mass spectrometry analysis of DltC species. Mass spectrometry result indicates purified DltC has a molecular weight of 9590 Da, which is equal to the calculated molecular weight of Ppant modified DltC, referred to as DltC(Ppant). **d,** SEC chromatography of WT and mutant DltB proteins. DltB mutants including V305D/I306D, S293A, H289A and H336A are properly folded, as they migrate predominantly as a monomeric peak similar with WT DltB.

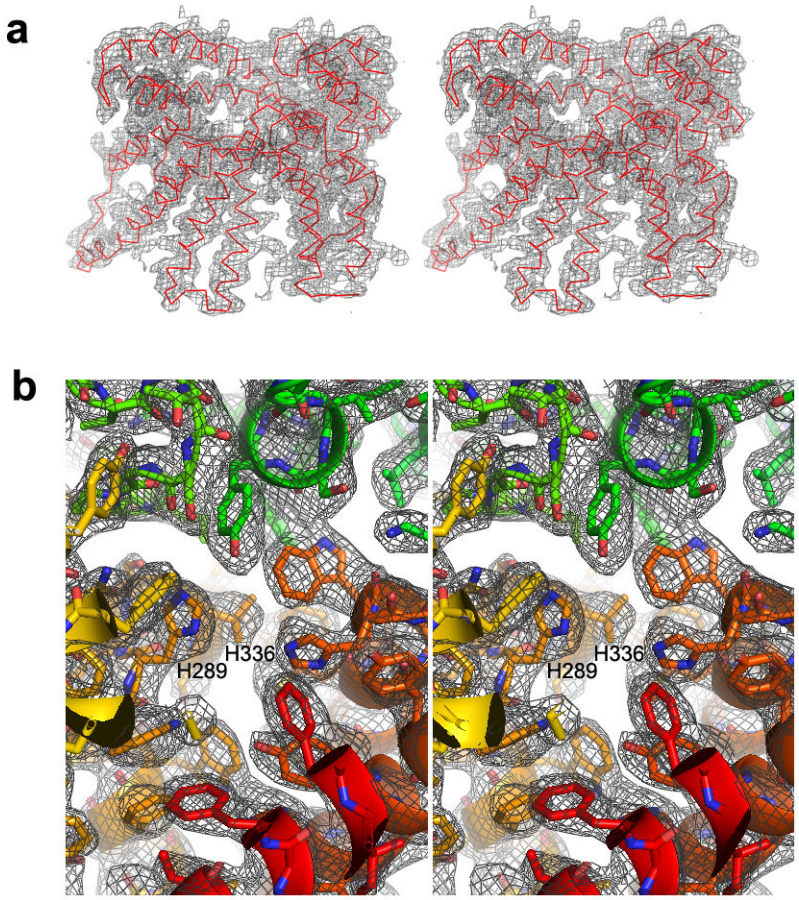

Extended Data Figure 3 |. Electron density map of DltB.

a, Stereo experimental electron density map, using phases derived from an Au-SAD phasing (Extended Data Table 1). This 2Fo-Fc map is contoured at 1.0δ. DltB backbone tracing is shown in red. **b,** The final 2Fo-Fc electron density map of the crystal form II (Extended Data Table 1). This map is contoured at 1.0δ, shown in stereo and in an orientation roughly looking down the funnel. Labeled along with the catalytic His336 is His289, another conserved residue (either His or Asn) among MBOAT proteins. Both His336 and His289 are located at the bottom of the extracellular funnel, and sandwich the top opening of the transmembrane tunnel.

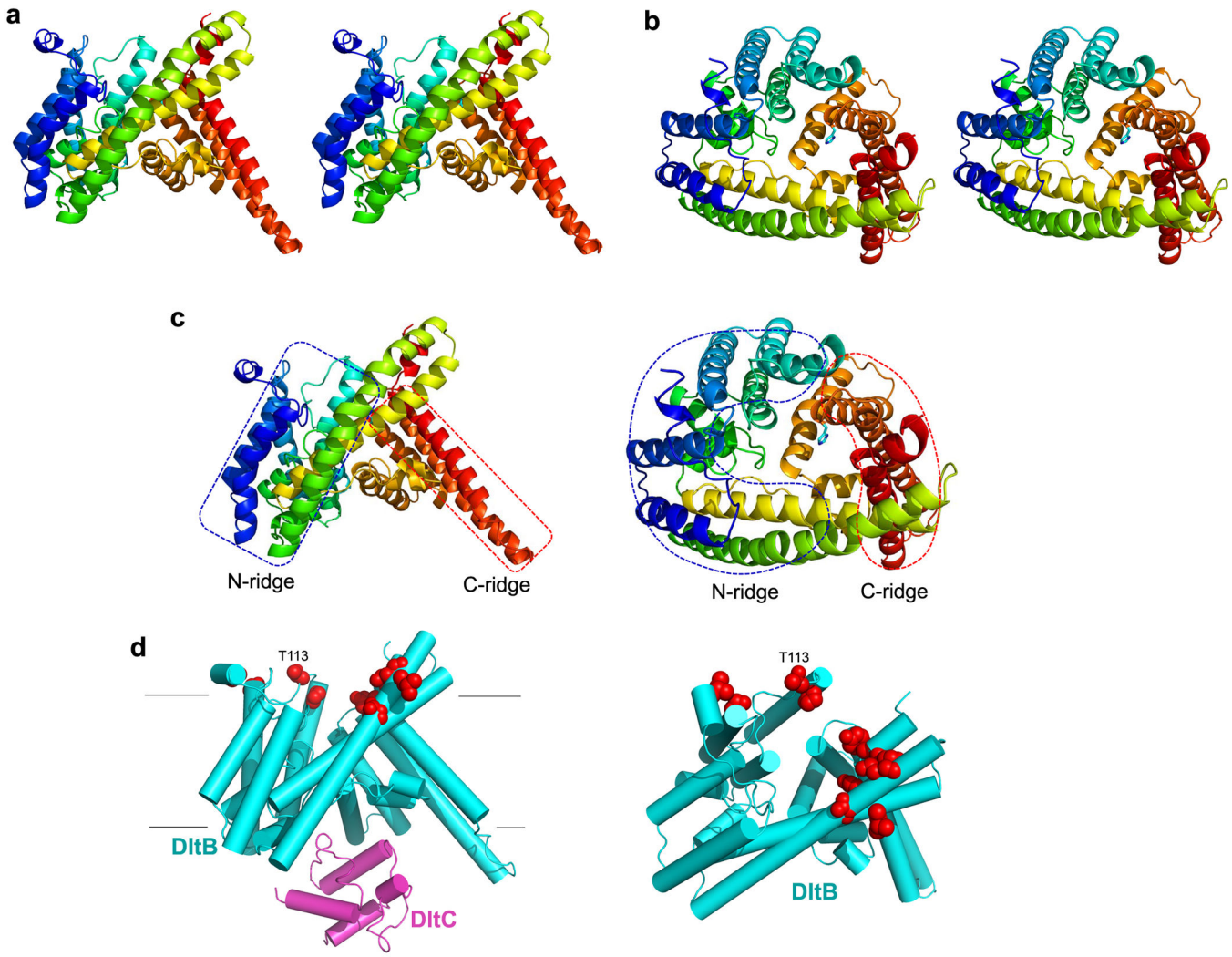

Extended Data Figure 4 |. Stereo view of DltB structure, and an extracellular "ring" of DltB residues associated with pathogen host switch.

a. The "front" side view of DltB (stereo view is provided). **b.** The "top" view of DltB, looking from extracellular space (stereo view is provided). The His336 sidechain is shown in sticks. The extracellular funnel is obvious with this angle. **c**. Cartoon illustration of the N- and C-ridges of DltB in two orthogonal views. **d.** Locations of host-pathogen sensitive sites in *S. aureus* DltB (I2, V61, T113, H121, I227, Q231, Y247, Y250, Y346, G401 and K402) are labelled with red balls in corresponding residues of the *S. thermophilus* DltB structure. It is obvious and striking that all 11 sites are located at apex of the extracellular ridge of DltB. *S. aureus* DltB T113 is not conserved and does not have the corresponding residue in other DltB (see Extended Data Fig. 5). Here the position of its closest residue is labelled. The intracellular DltC is shown in magenta. The DltB structure in these two panels are related with a 45° rotation.

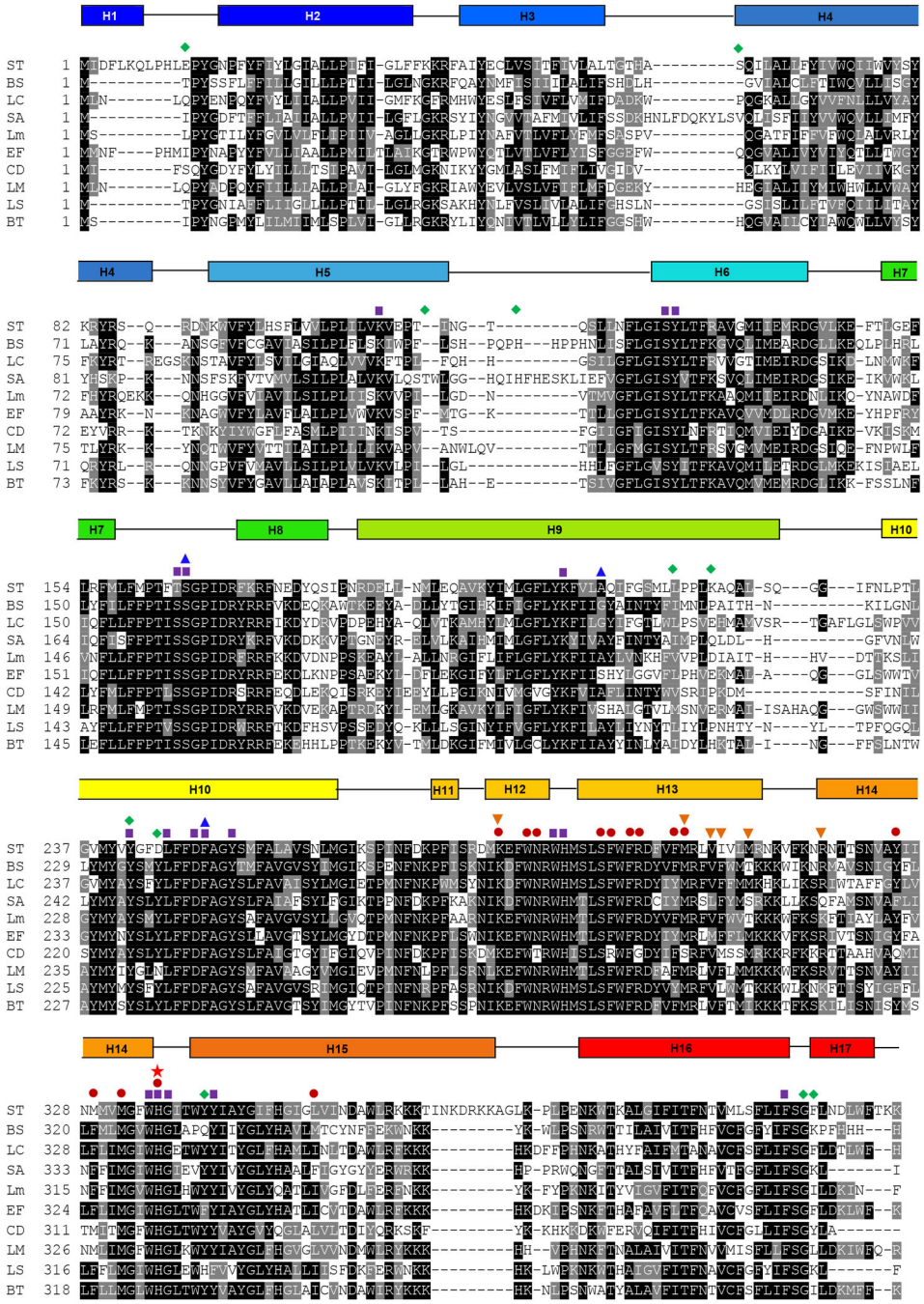

Extended Data Figure 5 |. DltB sequence alignment.

DltB sequences of representatives from 10 different genera of Gram-positive bacteria were chosen for sequence alignment using the T-Coffee server. Secondary structural elements of DltB are indicated above the alignment. Residues that form the funnel are identified by purple squares (■), and residues that form the tunnel are identified with dark red dots (●). DltB residues involved in direct interaction with DltC are indicated with orange inverted triangles (▼). Residues correspond to the three sites, single point mutation of which desensitize *S. aureus* to the inhibition by amsacrine, are indicated with blue triangles (▲).

Residues of *S. aureus* DltB, mutation of which convert host preference from human-specific to become capable of rabbit infection, are indicated with green diamonds (◆). A red star highlights the histidine residue that is completely conserved among MBOATs (★). Abbreviations: *Streptococcus thermophilus* (ST), *Bacillus subtilis* (BS), *Lactobacillus casei* (LC), *Staphylococcus aureus* (SA), *Listeria monocytogenes* (Lm), *Enterococcus faecalis* (EF), *Clostridioides difficile* (CD), *Leuconostoc mesenteroides* (LM), *Lysinibacillus sphaericus* (LS), *Brochothrix thermosphacta* (BT).

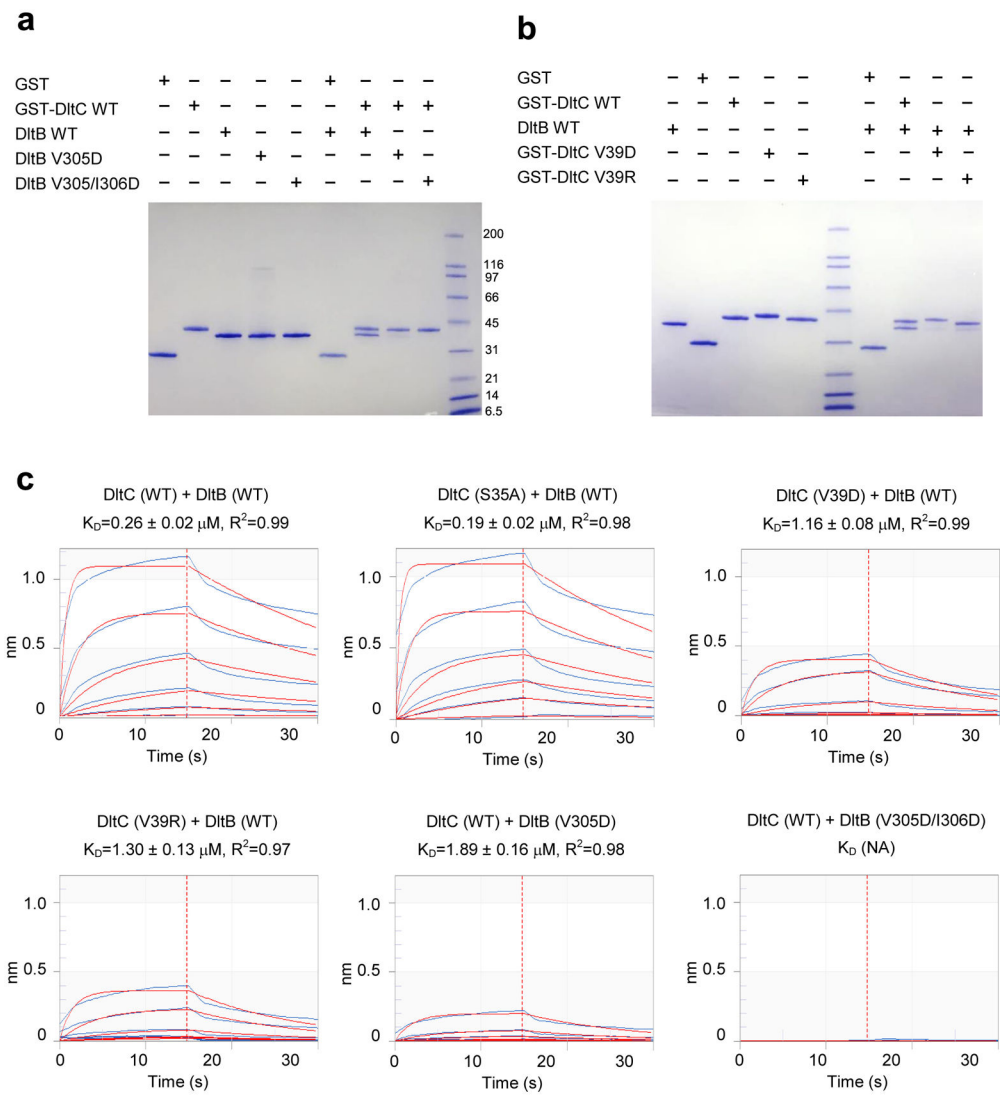

d

Samples in Octet Assay		K_D (μM)
GST-DltC	DltB	
WT	WT	0.26 ± 0.02
S35A	WT	0.19 ± 0.02
V39D	WT	1.16 ± 0.08
V39R	WT	1.30 ± 0.13
WT	V305D	1.89 ± 0.16
WT	V305D/I306D	NA

Extended Data Figure 6 |. GST-pulldown and Octet assays for analysis of the interaction between DltB and DltC(Ppant).

a, Results of using WT GST-DltC to pulldown either WT or mutant DltB, with GST to pulldown WT DltB as a negative control. Lanes of 1–5 show inputs in this experiment. Pulldown results demonstrate DltB and DltC can form stable complex at almost 1:1 molar ratio. DltB V305D lost most of its binding with WT GST-DltC, while the DltB double mutation V305D/I306D completely abolished the binding between DltB and DltC. **b,** Results of using WT or mutant GST-DltC to pulldown WT DltB. Lanes 1–5 show inputs in

this experiment. The GST-DltC V39D mutant runs slightly slower than WT GST-DltC and GST-DltC V39R on SDS-PAGE. Both of GST-DltC V39D and V39R mutants lost most of their binding with WT DltB. Pulldown experiments were performed at least twice technically, with the same results. **c**. Binding affinity measurements for DltB and DltC using Octet technique. WT and S35A GST-DltC show similar binding affinities with WT DltB. Mutation of residues on binding surface either on DltB or DltC can reduce or abolish their binding. Data are shown in blue, while the corresponding fits in red. DltB concentration gradient used here is: 0.03 μM, 0.1 μM, 0.3 μM, 1 μM, 3 μM, 10 μM. Octet assay were technically performed twice. **d,** Summary of Octet binding assay. WT and S35A GST-DltC show similar binding affinities with WT DltB. Kd values (mean) and Kd errors (SD) are shown for each assay. Mutation of residues on binding surface either on DltB or DltC can reduce or abolish their binding.

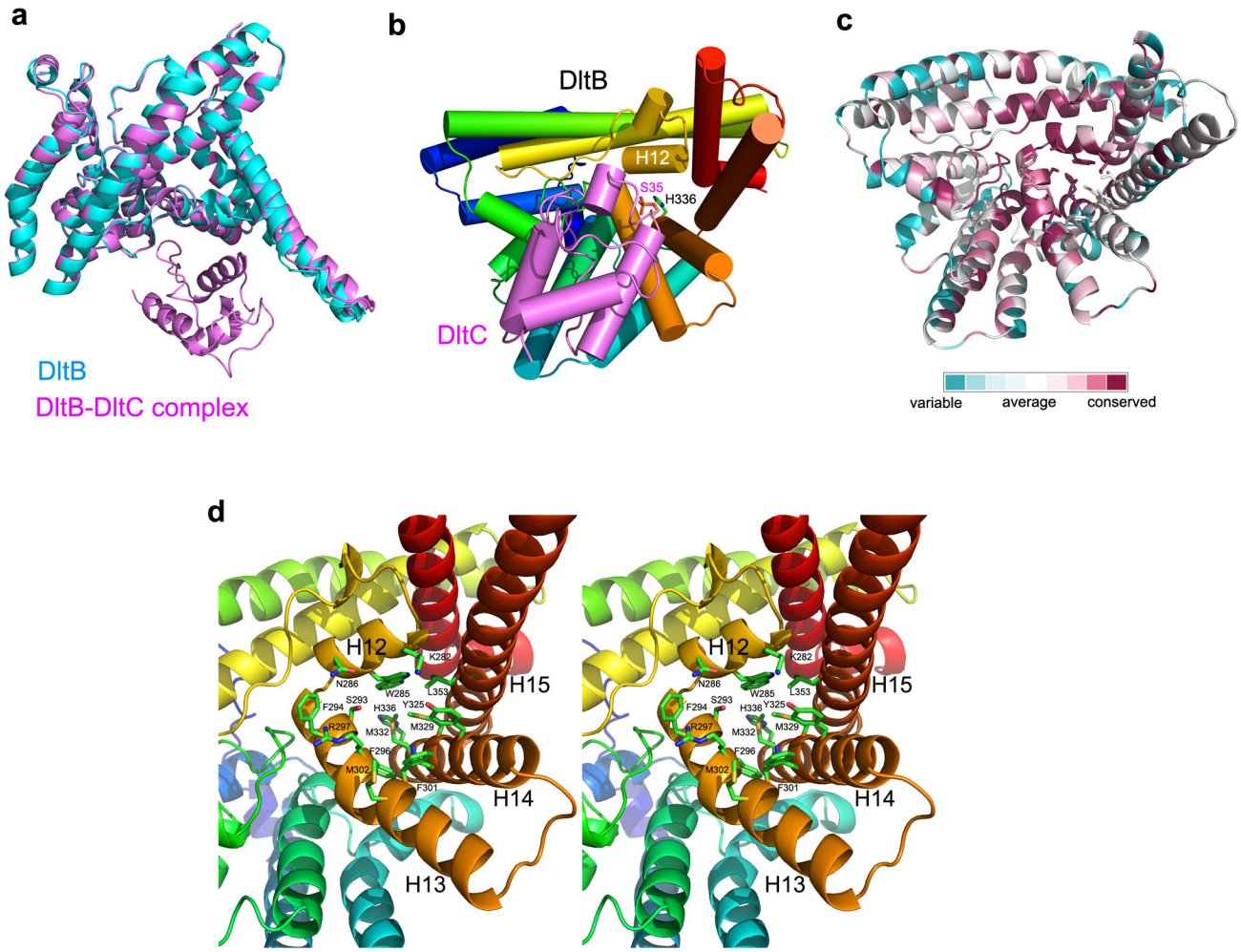

Extended Data Figure 7 |. Structural details of the DltB-DltC interface and the DltB tunnel. **a,** Superposition of crystal structures of DltB and the DltB-DltC complex. There is no significant conformational change in DltB upon DltC(Ppant) binding. **b,** Cylinder illustration of the DltB-DltC(Ppant) complex, viewed from the bottom of the DltB tunnel. DltB is colored in rainbow, while DltC is in purple. **c,** Conservation of the DltB tunnel region. Residues involved in tunnel formation are also highly conserved among DltB from different species (Extended Data Fig. 5). **d,** Stereo view of the DltB tunnel and residues forming this tunnel. The tunnel is formed by three helices from C-ridge (H13, H14 and H15) and the short H12 helix. Residues involved in tunnel formation in our structures are: Lys282, Trp285, Asn286, Ser293, Phe294, Phe296, Arg297, Phe301, Met302, Tyr325, Asn328, Met329, Met332, Leu353 and His336, which is also involved in the formation of extracellular funnel.

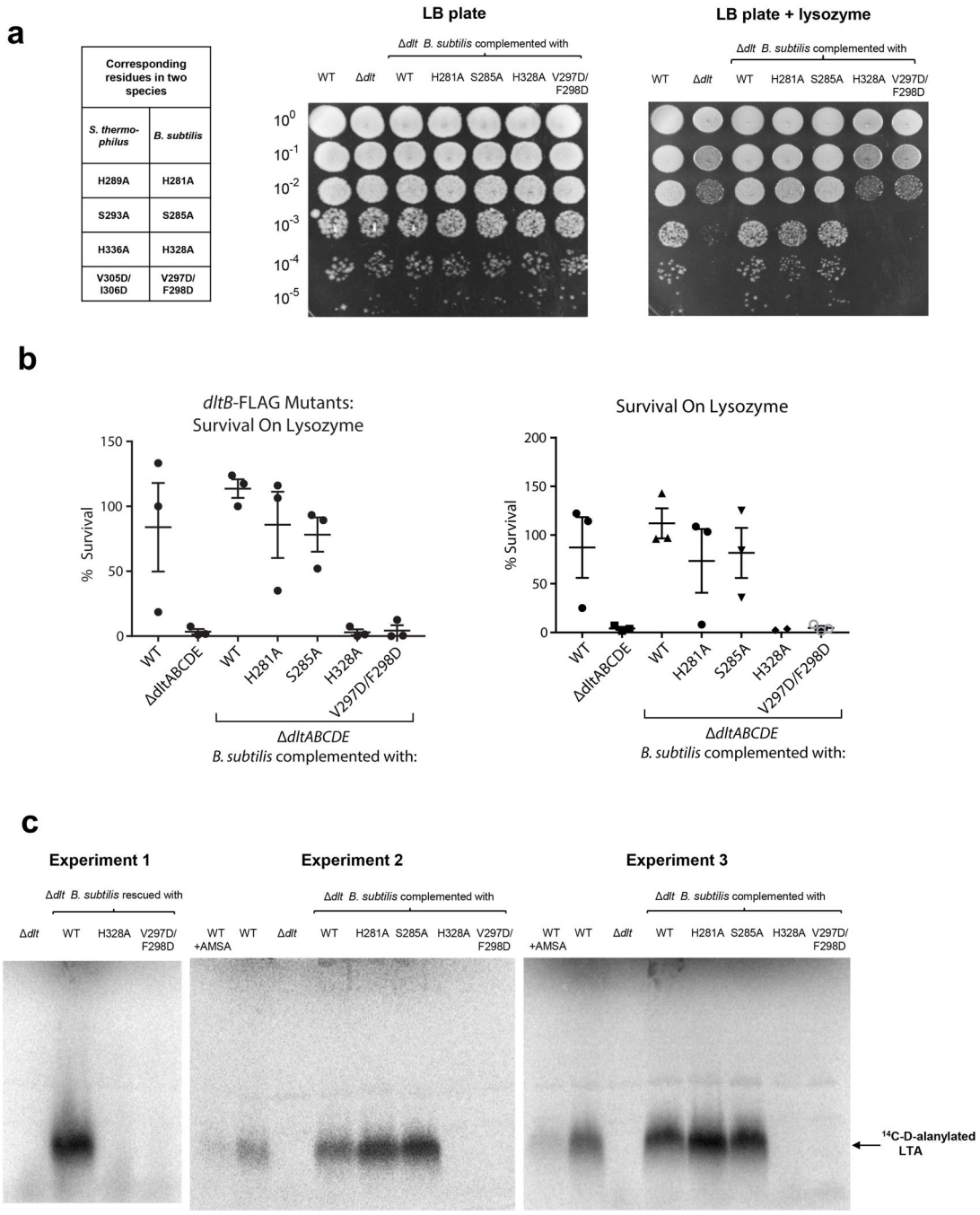

Extended Data Figure 8 |. Survival and LTA D-alanylation assays for WT and mutant DltB.

a, Lysozyme susceptibility survival assay. For DltB residues used in both LTA D-alanylation and survival assays, corresponding DltB residue numbers in two species are listed. The endogenous *dlt* operon was deleted in *B.subtilis* strain and complemented with an ectopic copy of the WT *dlt* operon without tag on DltB. Representative images of serial dilutions of cells plated on LB agar (left) and LB agar supplemented with 30 μg/ml of lysozyme (right). The genotype of the *dltB* gene is indicated above the corresponding column of serial dilutions. Dilutions of cells are indicated on the y-axis. Mutation of the critical histidine

(H328) and residues of DltB involved in binding with DltC (V297/F298) increase the susceptibility to lysozyme of *B. subtilis*. **b,** Percent survival of *B. bacillus* variants towards lysozyme treatment. It was calculated by dividing the colony forming units (CFUs) from lysozyme plates by the CFUs from LB only plates. Bars represent the means and error bars represent the standard deviations of three biological replicates. The genotype of *dltB* is indicated at the bottom. *B.subtilis* strains containing untagged DltB show similar lysozyme susceptibility pattern compared to those containing FLAG-tagged DltB. **c,** LTA D-alanylation assay. In experiment 1, the assay time was 120 min after ^{14}C-D-alanine was added, while for experiment 2 and 3, the assay time was 30 min. Experiment 2 and 3 are two parallel assays for LTA D-alanylation detection. AMSA represents amsacrine, a DltB inhibitor.

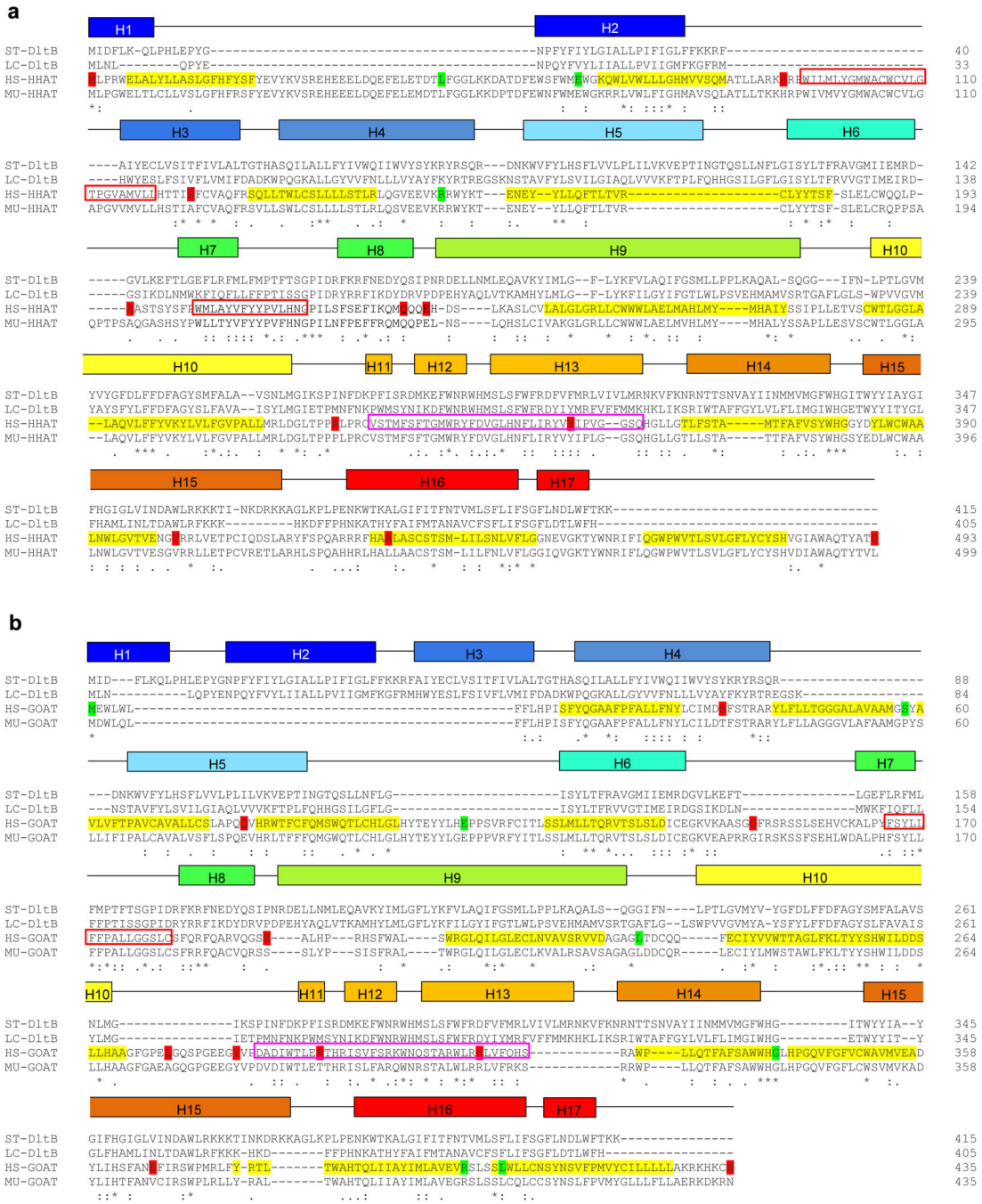

Extended Data Figure 9 |. Comparison and rationalization of topological data.

a. Comparison of HHAT topology data with DltB structure. **b.** Comparison of GOAT topology data with DltB structure. In both panels, secondary structures above DltB sequences are generated from our DltB crystal structure. Reported topology assignments of HHAT and GOAT were achieved using human proteins. Here we highlighted predicted HHAT/GOAT transmembrane helices for each protein with yellow background within sequences. Residues for human HHAT and GOAT that were experimentally verified to be located on cytoplasmic side are colored in red, and residues which are on luminal side are

colored in green. Helices and/or loops that are predicted to be associated with membrane surface or buried halfway within the membrane on the cytoplasmic side are indicated with red and magenta rectangles, respectively. It is obvious that the regions corresponding to DltB H7-H14 are topologically more conserved than those forming the DltB N- and C-ridges.

Extended Data Table 1 | Data collection, phasing and refinement statistics.

Every diffraction dataset was collected from a single crystal. Values in parentheses are for highest-resolution shell.

Data collection	**Crystal form I**		**Crystal form II**	**Crystal form III**
	Au-SAD	**Native**	**Native**	**Native**
Space group	$P2_1$	$P2_1$	$P2_1$	$P2_12_12$
Content per ASU	4 DltB + 3 DltC(Ppant)		4 DltB + 4 DltC(Ppant)	4 DltB
Wavelength (A)	1.02	1.00	1.00	1.00
Temperature (K)	100	100	100	100
Cell dimensions				
a, b, c (Å)	109.3, 122.0, 126.3	108.7, 121.1, 126.5	108.7, 124.6, 126.7	140.2, 242.1,96.2
α, β, γ(°)	90, 101.1, 90	90, 101.6, 90	90, 97.0, 90	90, 90, 90
Resolution (Å)	3.80 (3.87–3.80)	50.0–3.30 (3.40–3.30)	50.0–3.15 (3.24–3.15)	50.0–3.30 (3.40–3.30)
R_{sym}	0.152 (1.450)	0.170 (1.661)	0.165 (0.929)	0.115 (1.203)
$I/\sigma(I)$	19.0 (1.3)	13.1 (1.2)	8.6 (1.2)	11.5 (1.4)
$CC_{1/2}$	(0.626)	(0.732)	(0.582)	(0.563)
Completeness (%)	99.9 (99.4)	99.5 (98.7)	98.5 (87.8)	97.5 (98.1)
Redundancy	7.2 (6.5)	6.4 (6.3)	3.6 (2.9)	3.8 (3.2)
Refinement				
Resolution (Å)		50.0–3.30	50.0–3.15	50.0–3.30
No. reflections		46614	54118	47040
R_{work} / R_{free}		0.289 / 0.311	0.276 / 0.299	0.280 / 0.300
No. atoms				
Protein		15679	16308	13792
Ligand/ion		0	0	0
Water		0	0	0
B-factors				
Protein		86.6	45.1	108.9
Ligand/ion		N/A	N/A	N/A
Water		N/A	N/A	N/A
R.m.s. deviations				
Bond lengths (Å)		0.009	0.009	0.009
Bond angles (°)		1.409	1.338	1.400
Ramachandran plot				
Most favored (%)		94.9	96.6	96.1
Allowed (%)		5.1	3.4	3.9

Data collection	Crystal form I		Crystal form II	Crystal form III
	Au-SAD	Native	Native	Native
Disallowed (%)		0	0	0

Acknowledgements

We are grateful to the staff at ALS beamlines 5.0.1, 8.2.1 and 8.2.2 for assistance with synchrotron data collection. We thank Drs. Ning Zheng and Peter Hsu for comments on this manuscript, Dr. Thomas R. Hinds for discussion and advice on assays, Sergey Ovchinnikov for computational modeling, Loren Kruse for use of radioactive gel scanner, and Mark N. Ragheb for construction of the *dlt* operon deletion strain. This work was supported by NIH grant R01 GM127316 to W.X. and a Jane Coffin Childs postdoctoral fellowship to D.M. This work was also supported by CAS grant XDB08010303 to Z.R. and W.X., the NIGMS award DP2GM110773 to H.M. and the Bacterial Pathogenesis Training Grant 5T32AI055396-13 to K.S.L.

References

1. Hofmann K A superfamily of membrane-bound O-acyltransferases with implications for wnt signaling. Trends in biochemical sciences 25, 111–112 (2000). [PubMed: 10694878]
2. Chang TY, Chang CC, Ohgami N & Yamauchi Y Cholesterol sensing, trafficking, and esterification. Annual review of cell and developmental biology 22, 129–157 (2006).
3. Liu Q, Siloto RM, Lehner R, Stone SJ & Weselake RJ Acyl-CoA:diacylglycerol acyltransferase: molecular biology, biochemistry and biotechnology. Progress in lipid research 51, 350–377 (2012). [PubMed: 22705711]
4. Chang SC & Magee AI Acyltransferases for secreted signalling proteins (Review). Molecular membrane biology 26, 104–113 (2009). [PubMed: 19169935]
5. Masumoto N et al. Membrane bound O-acyltransferases and their inhibitors. Biochemical Society transactions 43, 246–252 (2015). [PubMed: 25849925]
6. Resh MD Fatty acylation of proteins: The long and the short of it. Progress in lipid research 63, 120–131 (2016). [PubMed: 27233110]
7. Tuladhar R & Lum L Fatty acyl donor selectivity in membrane bound O-acyltransferases and communal cell fate decision-making. Biochemical Society transactions 43, 235–239 (2015). [PubMed: 25849923]
8. Resh MD Palmitoylation of proteins in cancer. Biochemical Society transactions 45, 409–416 (2017). [PubMed: 28408481]
9. Lanyon-Hogg T, Faronato M, Serwa RA & Tate EW Dynamic Protein Acylation: New Substrates, Mechanisms, and Drug Targets. Trends in biochemical sciences 42, 566–581 (2017). [PubMed: 28602500]
10. Madan B & Virshup DM Targeting Wnts at the source--new mechanisms, new biomarkers, new drugs. Molecular cancer therapeutics 14, 1087–1094 (2015). [PubMed: 25901018]
11. Perego M et al. Incorporation of D-alanine into lipoteichoic acid and wall teichoic acid in Bacillus subtilis. Identification of genes and regulation. The Journal of biological chemistry 270, 15598–15606 (1995). [PubMed: 7797557]
12. Neuhaus FC, Heaton MP, Debabov DV & Zhang Q The dlt operon in the biosynthesis of D-alanyl-lipoteichoic acid in Lactobacillus casei. Microbial drug resistance 2, 77–84 (1996). [PubMed: 9158726]
13. Reichmann NT, Cassona CP & Grundling A Revised mechanism of D-alanine incorporation into cell wall polymers in Gram-positive bacteria. Microbiology 159, 1868–1877 (2013). [PubMed: 23858088]
14. Pasquina L et al. A synthetic lethal approach for compound and target identification in Staphylococcus aureus. Nature chemical biology 12, 40–45 (2016). [PubMed: 26619249]

15. Neuhaus FC & Baddiley J A continuum of anionic charge: structures and functions of D-alanyl-teichoic acids in gram-positive bacteria. Microbiology and molecular biology reviews: MMBR 67, 686–723 (2003). [PubMed: 14665680]
16. Peschel A et al. Inactivation of the dlt operon in Staphylococcus aureus confers sensitivity to defensins, protegrins, and other antimicrobial peptides. The Journal of biological chemistry 274, 8405–8410 (1999). [PubMed: 10085071]
17. Rios-Esteves J, Haugen B & Resh MD Identification of key residues and regions important for porcupine-mediated Wnt acylation. The Journal of biological chemistry 289, 17009–17019 (2014). [PubMed: 24798332]
18. Yang J, Brown MS, Liang G, Grishin NV & Goldstein JL Identification of the acyltransferase that octanoylates ghrelin, an appetite-stimulating peptide hormone. Cell 132, 387–396 (2008). [PubMed: 18267071]
19. Buglino JA & Resh MD Identification of conserved regions and residues within Hedgehog acyltransferase critical for palmitoylation of Sonic Hedgehog. PloS one 5, e11195 (2010). [PubMed: 20585641]
20. Das A, Davis MA & Rudel LL Identification of putative active site residues of ACAT enzymes. Journal of lipid research 49, 1770–1781 (2008). [PubMed: 18480028]
21. Lin S, Lu X, Chang CC & Chang TY Human acyl-coenzyme A:cholesterol acyltransferase expressed in chinese hamster ovary cells: membrane topology and active site location. Molecular biology of the cell 14, 2447–2460 (2003). [PubMed: 12808042]
22. McFie PJ, Stone SL, Banman SL & Stone SJ Topological orientation of acyl-CoA:diacylglycerol acyltransferase-1 (DGAT1) and identification of a putative active site histidine and the role of the n terminus in dimer/tetramer formation. The Journal of biological chemistry 285, 37377–37387 (2010). [PubMed: 20876538]
23. Viana D et al. A single natural nucleotide mutation alters bacterial pathogen host tropism. Nature genetics 47, 361–366 (2015). [PubMed: 25685890]
24. Jogl G, Hsiao YS & Tong L Structure and function of carnitine acyltransferases. Annals of the New York Academy of Sciences 1033, 17–29 (2004). [PubMed: 15591000]
25. Taylor MS et al. Architectural organization of the metabolic regulatory enzyme ghrelin O-acyltransferase. The Journal of biological chemistry 288, 32211–32228 (2013). [PubMed: 24045953]
26. Matevossian A & Resh MD Membrane topology of hedgehog acyltransferase. The Journal of biological chemistry 290, 2235–2243 (2015). [PubMed: 25488661]
27. Konitsiotis AD et al. Topological analysis of Hedgehog acyltransferase, a multipalmitoylated transmembrane protein. The Journal of biological chemistry 290, 3293–3307 (2015). [PubMed: 25505265]
28. Barnett BP et al. Glucose and weight control in mice with a designed ghrelin O-acyltransferase inhibitor. Science 330, 1689–1692 (2010). [PubMed: 21097901]
29. Ho SY & Keller TH The use of porcupine inhibitors to target Wnt-driven cancers. Bioorganic & medicinal chemistry letters 25, 5472–5476 (2015). [PubMed: 26522946]
30. Chen B et al. Small molecule-mediated disruption of Wnt-dependent signaling in tissue regeneration and cancer. Nature chemical biology 5, 100–107 (2009). [PubMed: 19125156]
31. Otwinowski Z & Minor W Processing of X-ray diffraction data collected in oscillation mode. Vol. 276 (Academic Press, 1997).
32. Adams PD et al. PHENIX: a comprehensive Python-based system for macromolecular structure solution. Acta crystallographica. Section D, Biological crystallography 66, 213–221 (2010). [PubMed: 20124702]
33. Zimmermann S et al. High-resolution structures of the D-alanyl carrier protein (Dcp) DltC from Bacillus subtilis reveal equivalent conformations of apo- and holo-forms. FEBS letters 589, 2283–2289, doi:10.1016/j.febslet.2015.07.008 (2015). [PubMed: 26193422]
34. Emsley P, Lohkamp B, Scott WG & Cowtan K Features and development of Coot. Acta crystallographica. Section D, Biological crystallography 66, 486–501 (2010). [PubMed: 20383002]

35. CCP4. The CCP4 suite: programs for protein crystallography. Acta Crystallogr. D 50, 760–763 (1994). [PubMed: 15299374]

36. DeLano WL & Brunger AT Helix packing in proteins: prediction and energetic analysis of dimeric, trimeric, and tetrameric GCN4 coiled coil structures. Proteins 20, 105–123. (1994). [PubMed: 7846022]

37. Ashkenazy H et al. ConSurf 2016: an improved methodology to estimate and visualize evolutionary conservation in macromolecules. Nucleic acids research 44, W344–350 (2016). [PubMed: 27166375]

38. Taly JF et al. Using the T-Coffee package to build multiple sequence alignments of protein, RNA, DNA sequences and 3D structures. Nature protocols 6, 1669–1682 (2011). [PubMed: 21979275]

39. Guariglia-Oropeza V & Helmann JD Bacillus subtilis sigma(V) confers lysozyme resistance by activation of two cell wall modification pathways, peptidoglycan O-acetylation and D-alanylation of teichoic acids. Journal of bacteriology 193, 6223–6232 (2011). [PubMed: 21926231]

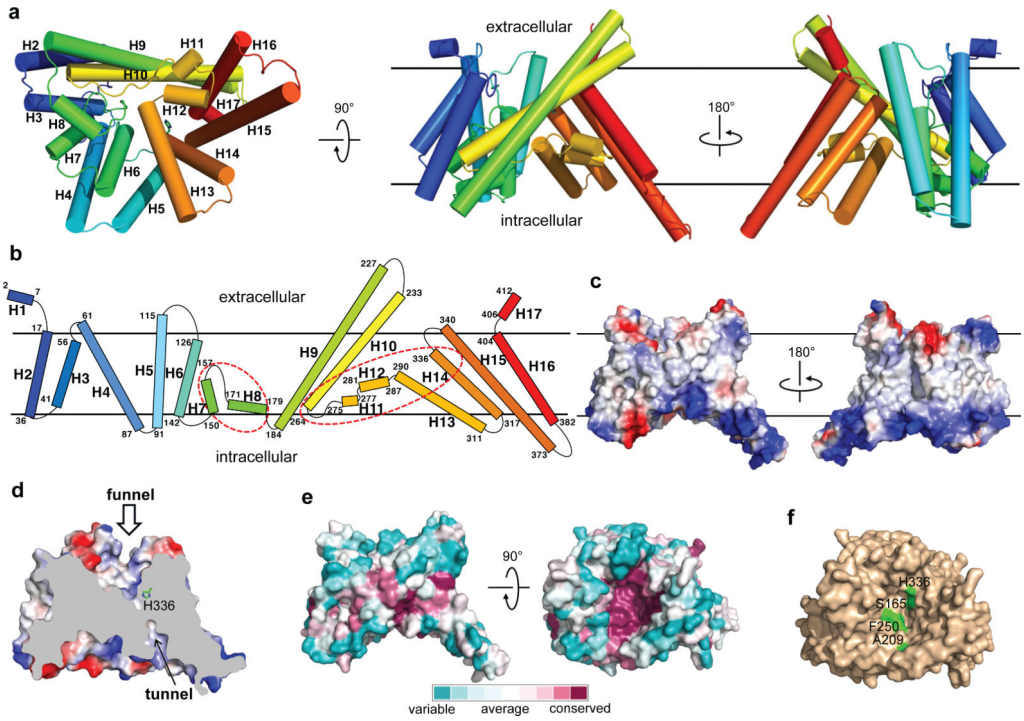

Figure 1 |. Overall structure of DltB and its conserved extracellular funnel.

a, The DltB crystal structure is shown in three orientations with rainbow colors: bottom, front and back (from left to right). **b,** Transmembrane topology cartoon of DltB. DltB contains a ring of 11 peripheral transmembrane helices, which shield a central thin layer (the structural core) highlighted by two red dashed circles. **c,** Electrostatic surface of DltB. **d,** A cut-away surface illustration showing the outward funnel connected with the cytosolic side through a tunnel. The histidine residue completely conserved among MBOATs (His336) is located at the bottom of the funnel. **e,** Striking conservation of the extracellular DltB funnel surface. Surface conservation pattern was generated based on sequence alignment shown in Extended Data Fig. 5. **f,** DltB top view showing the location of His336 and other three DltB residues (Ser165, Ala209 and Phe250), which when altered were found to desensitize *S. aureus* to the inhibition of LTA D-alanylation by amsacrine.

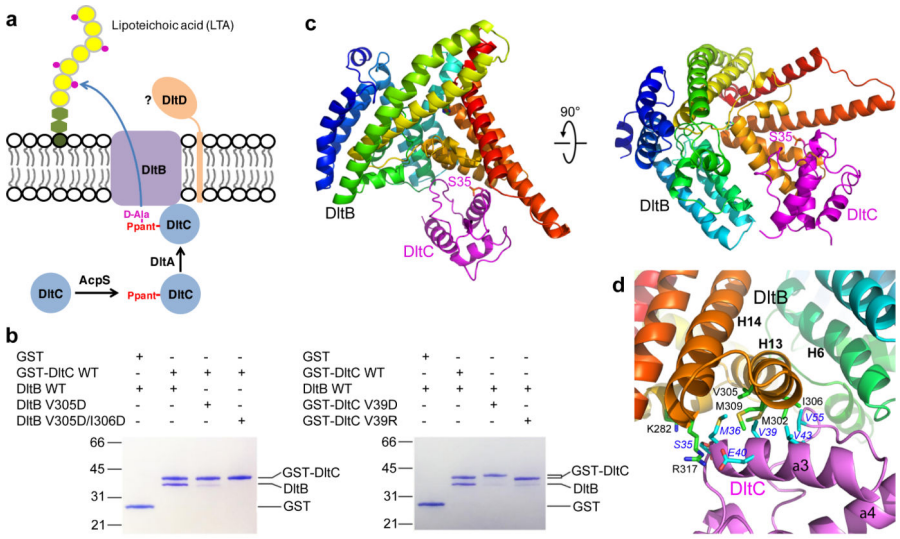

Figure 2 |. Structural basis of the DltB-DltC(Ppant) interaction.

a, Dlt proteins responsible for LTA D-alanylation in Gram-positive bacteria. Magenta dots on glycerophosphate units represent D-Ala moieties. **b,** Direct stable interaction between DltB and DltC(Ppant), and mutagenesis analysis of the DltB-DltC(Ppant) interface, as shown by GST-pulldown results. GST-pulldown experiments were performed at least twice with similar results. **c,** Overall structure of the DltB-DltC(Ppant) complex. DltC(Ppant) binds with DltB at cytosolic side, with the phosphate group of Ppant molecule which is attached on Ser35 of DltC pointing towards the DltB tunnel. **d,** The DltB-DltC(Ppant) interface. Side chains corresponding to DltB are shown as green sticks, while side chains of DltC are shown in cyan.

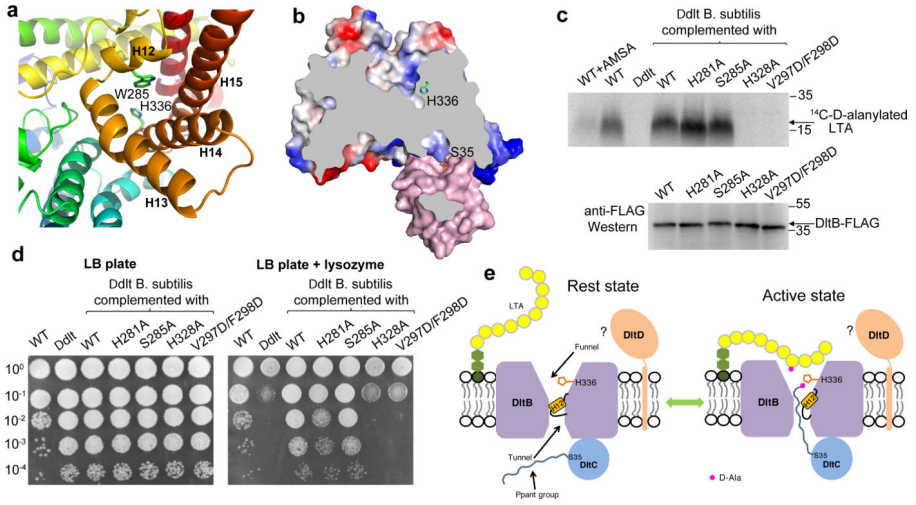

Figure 3 |. Structure of the DltB tunnel and the DltB-DltC(Ppant) binding mode provide insight into the molecular mechanism of DltB.

a, Residues forming the DltB tunnel. **b,** Cut-away surface illustration of the DltB-DltC(Ppant) complex. DltC(Ppant) pSer35 is located at the bottom of the tunnel. **c,** LTA D-alanylation assay. AMSA represents amsacrine, a DltB inhibitor. LTA D-alanylation assay were repeated for three times. H281, S285, H328 and V297/F298 in *B. subtilis* correspond to H289, S293, H336 and V305/I306 in *S. thermophilus*, respectively. **d,** Lysozyme susceptibility survival assay. Representative images are shown for serial dilutions of cells plated on LB agar (left) and LB agar supplemented with 30 μg/ml of lysozyme (right). Dilutions of cells are indicated on the y-axis. The survival assay was performed three times. **e,** A working model for DltB-mediated LTA D-alanylation. Cross-membrane D-alanylation is likely mediated by the DltB tunnel, whose opening/activation may be controlled by helix H12. The role of DltD in this reaction remains unclear.

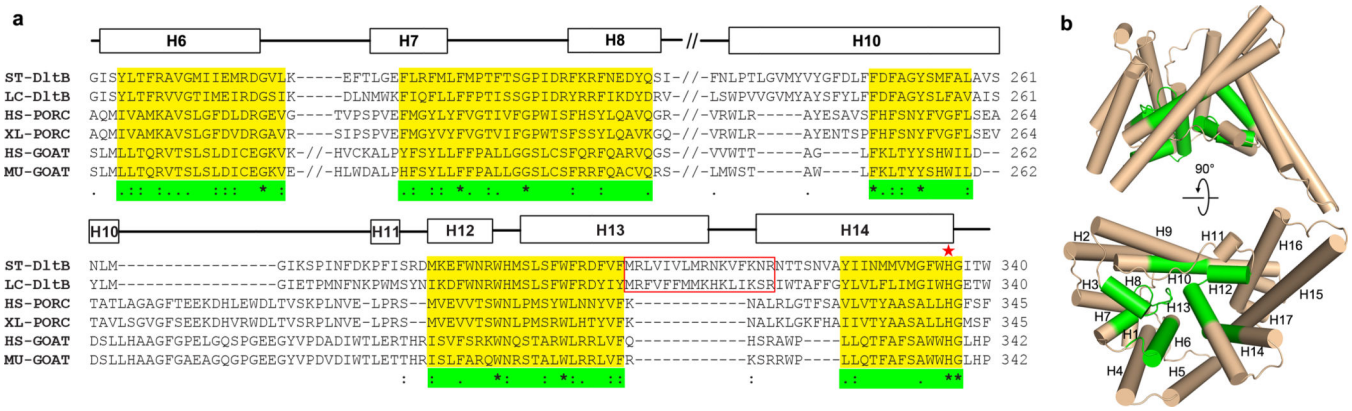

Figure 4 |. Conserved regions among bacterial DltB and vertebrate Porcupine/GOAT proteins.

a, Alignment of conserved regions of DltB, Porcupine (PORC) and GOAT. Conserved sequences are highlighted in yellow (and in green under the sequences). The red rectangle indicates the DltB-specific insertion, which is involved in the binding of DltC(Ppant). A red star marks the most conserved histidine residue among MBOATs. Abbreviations: *Streptococcus thermophilus* (ST), *Lactobacillus casei* (LC), *Homo sapiens* (HS), *Xenopus laevis* (XL), *Mus musculus* (MU). **b,** Conserved MBOAT core. Conserved regions among MBOATs form a central core in DltB structure (colored in green), whereas the peripheral helices shielding the core are largely non-conserved (colored in wheat).